ACS APPLIED MATERIALS & INTERFACES

RESEARCH ARTICLE

www.acsami.org

Vanadium Oxide Nanotube Spherical Clusters Prepared on Carbon Fabrics for Energy Storage Applications

Sanjaya D. Perera, Bijal Patel, Jeliza Bonso, Max Grunewald, John P. Ferraris, and Kenneth J. Balkus, Jr.*

Department of Chemistry and the Alan G. MacDiarmid Nanotech Institute, The University of Texas at Dallas, 800 West Campbell Road, Richardson, Texas 75080, United States

ABSTRACT: Vanadium oxide nanotubes have shown great promise as electrode materials for energy storage devices. In this study, we report the synthesis of V_2O_5 nanotube (VNT) clusters, which form densely packed radial arrangements of VNTs on high-surface-area carbon fiber fabrics (CF). This was achieved by coating the CF with V_2O_5 by pulsed laser deposition (PLD). Hydrothermal treatment of the PLD films in the presence of excess intercalated V_2O_5 results in formation of well-adhered VNT clusters on the CF. The densely packed VNTs have inner and outer diameters and interlayer distances of ~24, ~70, and ~2.4 nm, respectively. Coin cell type supercapacitors (CR2032) were assembled using VNT-CF as the anode material and electrochemical properties were evaluated.

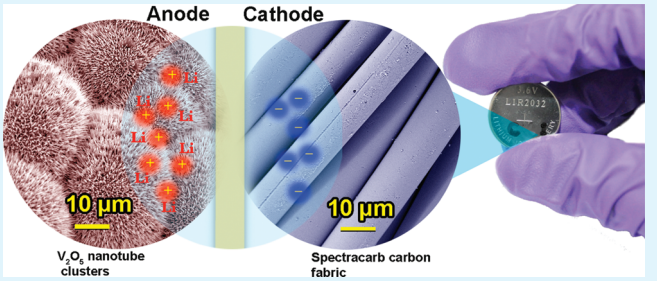

KEYWORDS: V_2O_5 nanotubes, nanotube spherical clusters, nanourchins, pulsed laser deposition, supercapacitors

INTRODUCTION

There is growing interest in new energy storage devices that are low cost, lightweight, and deliver high energy and power densities. Energy storage devices based on nanostructured electrodes are lightweight and display much larger power densities than conventional batteries and higher energy densities compared to conventional capacitors. Electrochemical capacitors have been studied intensively and rely mainly electrochemical double-layer capacitance (EDLC) or pseudocapacitance, which are known to have high power and high energy density, respectively. Supercapacitors are special type of energy storage device, which display intermediate power and energy, between dielectric capacitors and electrochemical batteries. Such devices can deliver high power during shorter periods of time, making them attractive for electric automobile applications that require quick bursts of energy.[1] Currently, carbon-based electrodes and metal oxides are mainly associated with supercapacitor electrodes. Carbon-based supercapacitor technology has become the cheapest technology because of the low production cost of activated carbon. These systems store charges on the surface of electrodes based purely on an electrochemical double layer. Unlike charge transfer reactions that occur in electrochemical batteries where charges are generated in the structure of the material, EDLCs deliver charges at much faster rates with high power densities. However, the charged species adsorbed on the carbon material are only on the surface and the energy density of this type of capacitor is limited by the accessible surface area. Metal oxide based electrodes are known to exhibit charge transfer reactions and generate a large number of charges within the structure. Hence, they can exhibit higher energy densities than EDLCs, but because of the slow charge transfer kinetics of metal oxide based electrodes, they exhibit much lower power densities than EDLCs. Up to now, many different types of metal oxides (RuO_2, MnO_2, NiO, V_2O_5) have been employed in supercapacitors.[2−5] In recent years, Ru-based electrodes have shown promise and offer higher specific capacitance and higher power densities.[6] However, the high cost of Ru based materials has greatly limited commercial energy storage applications. As a low-cost alternative to RuO_2, vanadium oxides have been shown to be promising candidates for energy storage applications. Besides changing the electrode material, increasing the surface area of the electrode is one of the key strategies to increase the number of active sites where charges are stored. Low dimensional nanostructures such as nanotubes,[7−9] nanowires and nanobelts[10,11] exhibit higher surface area and novel physiochemical properties compared to bulk materials.[12,13] The nanostructures having a tubular morphology are particularly attractive for electrode materials since there are three different contact regions available: inner, outer, and tube ends, which creates short diffusion pathways for ions.[14] In recent studies, low-dimensional nanostructures of vanadium oxides have shown outstanding electrochemical properties suitable for energy storage devices. The lamellar structure of vanadium oxide nanotubes improves the Li^+ ion loading due to the lower diffusion distance and higher surface area for intercalation compared with bulk V_2O_5.[10,15] In addition to the higher Li ion diffusion coefficient, there are several accessible oxidation states for vanadium (V^{2+}, V^{3+}, V^{4+}, V^{5+}) for electrochemical redox reactions. The ease of reducing from the +5 oxidation state to lower oxidation states and the ability to intercalate Li ions into the layered structures makes V_2O_5

Received: September 4, 2011
Accepted: October 26, 2011
Published: October 26, 2011

an ideal material for faradaic capacitors and high-energy Li ion batteries.[16,17]

Vanadium oxide nanotubes have been synthesized by several methods, such as nonalkoxide routes,[18] and the sol−gel reaction of vanadium alkoxides with a primary amine.[19,20] While there has been progress in controlling the morphology of V_2O_5 nanostructures, growing of these V_2O_5 nanostructures as thin films remains a challenge. In earlier reports, vanadium oxide thin films have been made by sputtering,[21] evaporation,[22] vapor deposition[23] and pulsed laser deposition (PLD).[24,25] We have previously demonstrated the preparation of low-density metal oxide thin films and nanostructures by PLD for different applications.[26,27] Furthermore, electochromic devices,[28] lithium ion microbatteries,[29] and photochromic devices[30] have also been prepared from laser ablated V_2O_5 thin films. The formation of VNT thin films by PLD has not been reported before.

Although the various nanostructured forms of V_2O_5 have shown improved electrochemical properties,[31−33] the low electronic conductivity of V_2O_5 requires the combination of V_2O_5 with conductive substrates, such as conductive polymers[34,35] or carbonaceous materials.[36,37] Supporting V_2O_5 on a high-surface-area carbon based material is particularly attractive because of the potential for increasing both the conductivity and the capacitance of the composite relative to the metal oxide or carbon itself. Recently we reported V_2O_5 nanowire/carbon nanotube composites for supercapacitor applications and observed that the presence of CNTs improves the power and energy densities.[38] Fang and co-workers also reported the fast and reversible surface reduction of V_2O_5 dispersed on carbon nanotubes.[39] Additionally, Chen et al. investigated the capacitive properties of a activated carbon/V_2O_5 composite.[40]

In this paper, a novel method for the preparation of three-dimensional (3D) VNT clusters on commercially available high surface area carbon fabric via PLD is reported for the first time. The PLD technique was employed to deposit vanadium oxide thin films on conductive carbon fiber sheets followed by a hydrothermal treatment to grow the VNT spherical clusters on the carbon fibers. As-prepared 3D VNT clusters on high surface area carbon fabric showed promising electrochemical properties for supercapacitor applications. The VNT films were characterized by XRD, infrared (IR), and Raman spectroscopy, as well as scanning electron microscopy (SEM) and transmission electron microscopy (TEM).

EXPERIMENTAL SECTION

Materials. All reagents were used without further purification. Vanadium pentoxide (99%) was purchased from Sigma-Aldrich. Hexadecylamine (HDA) was obtained from Alfa-Aesar. All solvents were used as received. Carbon fiber fabric (Spectracarb^{TM} 2225) and carbon fiber sheet (Spectracarb^{TM} 2250A) were purchased from Engineered Fiber Technology (Shelton, CT). Lithium bis(trifluoromethanesulfonamide) (LiTFSI) was obtained from TCI America. A Teflon film (Gore Company) was used as the separator between the two electrodes.

Deposition of V_2O_5 Thin Films. The Spectracarb substrates were cleaned by sonication in deionized water and ethanol. Thin films of V_2O_5 nanoparticles were deposited on the Spectracarb by PLD as follows. First 2.5 g of V_2O_5 powder were pressed into a pellet with a diameter of ∼2.5 cm and a thickness of ∼3 mm. Under a controlled atmosphere (∼200 mTorr of oxygen) V_2O_5 was deposited on a Spectracarb fabric at 300 °C. The pulsed laser deposition was performed for 60 min using a Lambda Physik Compex 102 excimer laser operating at 248 nm (KrF) and 300 mJ with a repetition rate of 10 Hz. The laser beam was focused onto the target at an angle of 45°. The target was rotated at 5 rpm.

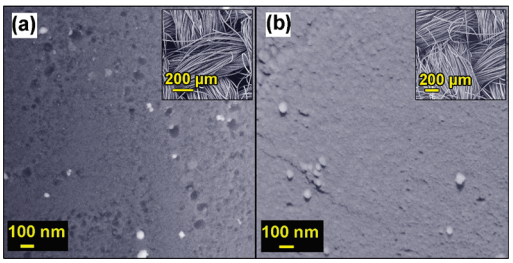

Figure 1. High-resolution SEM images of the surface of a carbon fiber in fabric (a) before and (b) after the pulsed laser deposition of V_2O_5. Inset images show the low-resolution images of carbon fiber fabric before and after the pulsed laser deposition.

VNT films were synthesized by modification of a published procedure.[21] A suspension of V_2O_5 (10 mmol) and 1-hexadecylamine (HAD) in 20 mL of deionized (DI) water was stirred for 2 h at room temperature. DI water (20 mL) was added to the mixture and stirred for 48 h to yield a dark yellow suspension. The resulting suspension and the PLD V_2O_5/Spectracarb fabric were sealed in a Teflon-lined autoclave and heated at 180 °C for 7 days. The VNT clusters grown on the Spectracarb (VNT-CF) fabric were washed with deionized water then ethanol and dried at 80 °C.

Supercapacitor Assembly. A typical coin cell packaging (CR2032) was used to assemble the asymmetric supercapacitor. The VNT-CF electrode served as the anode and the blank Spectracarb carbon fabric as the cathode, which were separated by a Teflon sheet. In order to have a better electrode contact with the coin cell metal contacts, two carbon fiber sheet spacers (Spectracarb 2250A) were sandwiched between each electrode and the stainless steel current collectors (spacers). Lithium bis(trifluoromethanesulfonyl)imide (LiTFSI) in dry acetonitrile (0.1M), was introduced and sealed in the coin cell using a crimper (Shenzhen Yongxingye Precision Machinery mold) compressing at 1500 psi.

Characterization. Transmission electron microscope (TEM) and scanning electron microscope (SEM) images were acquired using a JEOL JEM-2100 TEM at 200 kV (JEOL Co. Ltd.) and a Leo 1530 VP field emission electron microscope respectively. X-ray powder diffraction (XRD) patterns were obtained using a Rigaku Ultima III diffractometer (Cu Kα radiation). Fourier transform infrared (FT-IR) spectra were recorded from a Nicolet Avatar 360 FT-IR spectrophotometer. Cyclic voltammograms and galvanostatic charge discharge profiles were obtained using a supercapacitor testing system (SCTS, Arbin Instruments) in the potential range of −0.5 to 1.5 V.

RESULTS AND DISCUSSION

The key to growing V_2O_5 nanotubes on the high surface area carbon substrates was the deposition of a thin layer of V_2O_5 nanoparticles by PLD. Figure 1 shows the SEM images of the surface of the carbon fiber before (a) and after (b) pulsed laser deposition of V_2O_5 thin film. The inset low-resolution SEM images show the arrangement of carbon fibers in the fabric. The thin layer of deposited V_2O_5 on these carbon fibers acts as a seed layer for the growth of VNT clusters. Orthorhombic α-V_2O_5 has a layered structure, which is built from stacking of distorted edge-shared VO_5 pyramids in the (010) direction. There are singly coordinated vanadyl oxygens, doubly coordinated and bridging oxygens triply coordinated to vanadium ions.[17] The first step in the synthesis of the V_2O_5 nanotubes is the intercalation of hexadecylamine (HDA), which forms a loosely interconnected sheet structure. This was achieved by

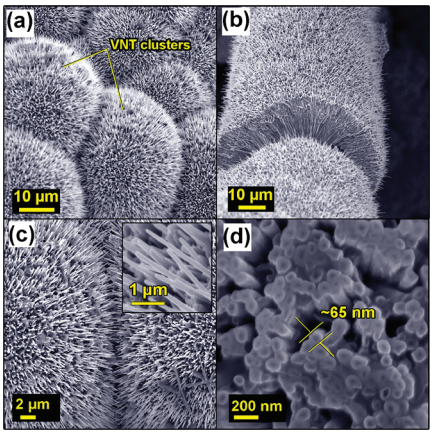

Figure 2. (a, b) Spherical clusters of densely packed VNTs grown on carbon fibers of Spectracarb carbon fabric. (c) Boundary of two clusters consists of radially grown nanotubes, inset image shows nanotubes are freely formed and attached from one end. (d) Open-end tubular structure of V_2O_5 nanotubes in a spherical cluster.

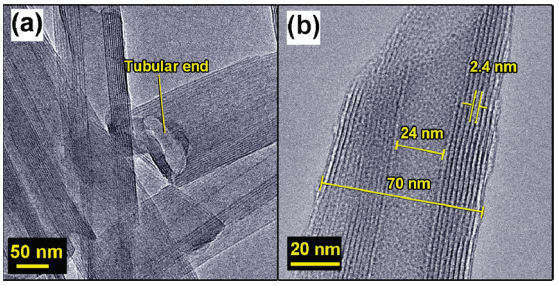

Figure 3. High-resolution TEM micrographs for VNTs. (a) Tubular structure is formed by scrolling few layers of nanosheets to give the hollow center extend toward the end of the nanotube. (b) Layered structure of VNTs show 2.4 nm lattice distance with outer and inner diameter of 70 and 24 nm, respectively.

vigorous stirring of V_2O_5 in the presence of HDA. During the hydrothermal treatment the HDA intercalated V_2O_5 layers delaminates which fascilitates scrolling of the sheets to form the tubular structure. Previously O'Dwyer et al. synthesized spherical nanotube clusters and discussed the possible mechanism involved in growing of VNT urchins.[33] Moreover, it was suggested that the linking of lamina structure in the presence of the amines. In present study, the delaminated V_2O_5 layers may anchor to the PLD film V_2O_5 surface and the excess HAD surfactant may fascilitate the radial arrangement of VNTs in the same way. Additionally, the densely packed, laser-deposited V_2O_5 nanoparticle layer may anchor the scrolling lamellars, resulting in partially oriented nanotubes. We have observed this with high-aspect-ratio zeolite crystal films grown by this PLD process.[27]

The SEM images in Figure 2 show the morphology of the VNT clusters and nanostructure of VNT films grown on the carbon fabric. The radially grown VNT clusters with densely packed nanotubes form spherical three-dimensional structures (Figure 2a). In some cases, the VNTs grow radially along the fiber axis (Figure 2b). Images c and d in Figure 2 further illustrate the morphology of the V_2O_5 nanotubes at higher magnification with an average diameter of ~70 nm (Figure 2d). The excess V_2O_5 in the hydrothermal medium results in some free VNTs, which have similar dimensions to the VNT clusters supported on the carbon fibers. The dark black-green color of the nanotubes in clusters and the free VNTs in the reaction medium is an evidence of partial reduction of V^{5+} to

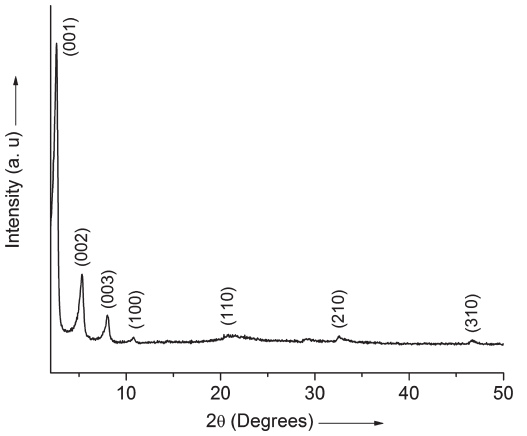

Figure 4. X-ray diffraction pattern of as-made VNTs on carbon fiber fabric.

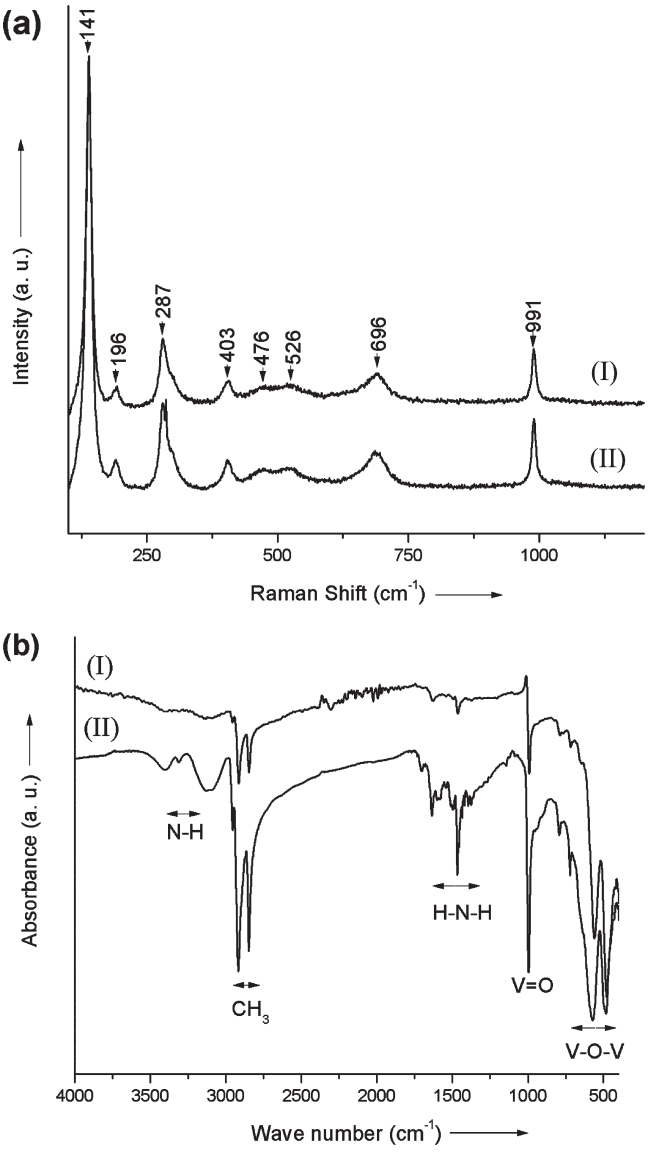

Figure 5. (a) Raman and (b) FT-IR spectra of the VNT clusters (I) and the bulk (II) VNTs.

dx.doi.org/10.1021/am2011965 |ACS Appl. Mater. Interfaces 2011, 3, 4512–4517

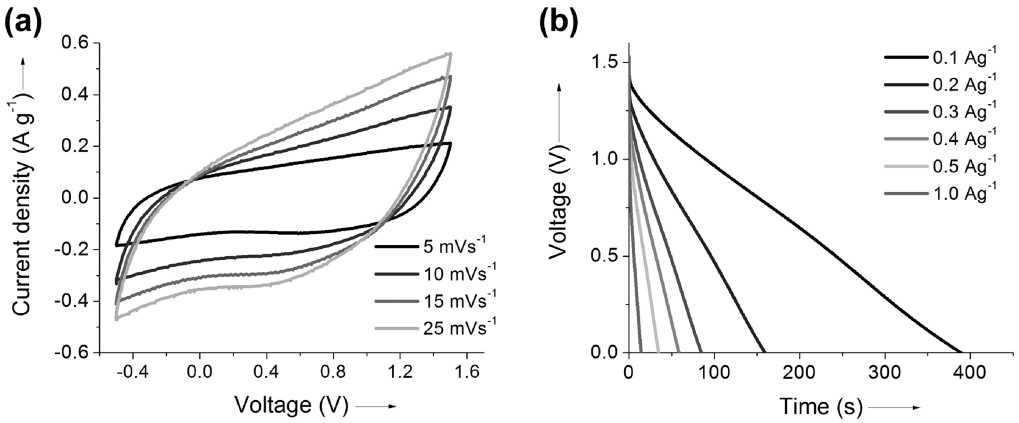

Figure 6. (a) Cyclic votammograms at different scan rates and (b) Galvanostatic discharge curves of VNT-CF electrode for various current densities from 0.1 to 1.0 Ag^{1-}.

V^{4+} during hydrothermal synthesis. This has previously been observed for V_2O_5 nanostructures prepared under similar conditions.[5,10,38]

The transmission electron microscopy (TEM) images shown in Figure 3 reveal open-ended vanadium oxide nanotubes (Figure 3a). These open ended nanotubes are ~70 nm in diameter with ~24 nm pores, which is consistent with the SEM images (Figure 2d). The dark fringes of the layered structure with the interlayer distance ~2.4 nm in Figure 3b correspond to V−O layers and light fringes are interlayer spacing of V−O layers, which contain intercalated primary amines.[41]

The X-ray diffraction patterns of V_2O_5 nanotubes and VNT films are shown in Figure 4. The (001), (002), (003), (100), (110), (210), and (310) reflections are consistent with the crystalline V_2O_5 monoclinic phase.[42−44] The most intense peak at $2\theta = 2.56°$ angle is the (001) reflection corresponding to a *d*-spacing of ~3.4 nm. This value is a little larger than the interlayer spacing measured by the TEM image (~ 2.4 nm) depicted in Figure 3b. This difference is may be due to the dehydration and partial rearrangement of the template between the layers upon exposure to the high-voltage electron beam under the ultrahigh-vacuum conditions used in TEM analysis.[10] The interlayer distance of the as-synthesized nanotubes with HDA template is similar to the previously reported *d*-spacing of VNTs prepared using HDA template.[45,46] Moreover, the *d*-spacing is larger than the amine molecular length (2.12 nm), suggesting the intercalation of the amines between the nanotube walls, which are formed with the double layer of VO_4 tetrahedra.[33,42]

The as-prepared VNT clusters and free VNTs were further analyzed by Raman and FT-IR spectroscopy (Figure 5). The strong Raman bands located at 197 and 196 cm^{-1} are attributed to the bending mode of $(V_2O_2)_n$ and chain translation, which is associated with the layered structure (Figure 5a). The Raman band at 991 cm^{-1} is due to the terminal oxygen (V═O) stretching mode. The peak at 696 cm^{-1} corresponds to the doubly coordinated oxygen (V_2−O) stretching mode, which is due to corner-shared oxygen common to two pyramids. The peak at 526 cm^{-1} is attributed to the triply coordinated oxygen (V_3−O) stretching mode of edge-shared oxygen in common with three pyramids. Bands at 403 and 476 cm^{-1} correspond to the bending vibrations of the bridging a V−O−O). Two lower frequency peaks at 196 and 287 cm^{-1} are results from the bending vibrations of the V═O bonds.[47,48]

The FT-IR spectra in Figure 5b show strong bands at 2917 and 2849 $cm^{-1}$for the C−H stretching and bending modes of the intercalated HDA template. The H−N−H wagging vibrations of alkylammonium ions adsorbed on V_2O_5 are shown between 1500 to1650 cm^{-1}. Vanadyl oxygen (V═O) stretching V−O−V bending modes at 1005, 578, and 485 cm^{-1} exhibits the most important structural evidence of

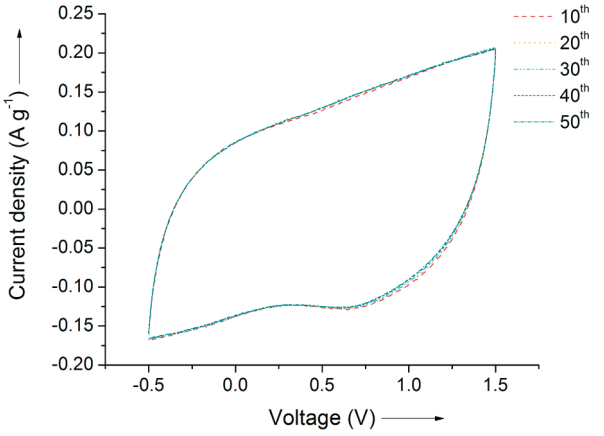

Figure 7. Cyclic voltammograms of the VNT-CF electrode for 50 continuous cycles acquired at 5 mVs^{-1} scan rate (only 10th −50th cycles were plotted).

the presence of VNTs with vibrational modes of ν_s(V═O), ν_s-(V−O−V), and ν_{as}(V−O−V), respectively.[20]

The electrochemical properties of the as-prepared VNT-CF electrode were studied by assembling coin cell type supercapacitors (CR2032) in a two-electrode system. The as-prepared VNT-CF electrode was employed as the negative and a carbon fiber fabric was used as the positive electrode. Figure 6a shows the cyclic voltammetric response of the VNT-CF in 1 M LiTFSI (in acetonitrile) at different scan rates in the potential range from −0.5 to 1.5 V. The quasi-rectangular shape in Figure 6a indicates a balance of pseudo capacitance from the V_2O_5 and EDLC from carbon fiber fabric. The retention of the shape of the cyclic voltammograms even at 20 mVs^{-1} is a good indication of reversible Li ion intercalation. During the charging process V^{+5} ions are reduced to V^{+4} in the lattice, resulting in intercalation of Li ions from the electrolyte to balance the overall charge. As previously reported, the V^{4+} ions are partially oxidized to V^{5+}, leaving a mixture of V^{4+} and V^{5+}. Volumetric changes due to the difference in the sizes of these ions, 0.86 Å versus 0.495 Å and the formation of defects in the lattice structure allows more freedom for Li^+ ion intercalation and deintercalation.[17,49] The high porosity of the carbon fiber fabric facilitates the mobility of Li^+ ions back and forth during the redox cycle. Galvanostatic discharge cycles of the VNT-CF electrode at different current densities from 0.1 to 1.0 A g^{-1} are shown in Figure 6b. The nearly straight line for the discharge profile further suggests balanced redox and electric double layer properties of

the VNT-CF electrode. The energy and power densities were calculated according to the equation $E = (I\Delta t\Delta V)/(2m)$ and $P = E/\Delta t$, where I is the constant discharge current, Δt is the discharge time, ΔV is the voltage difference after the voltage drop and m is the total mass of both electrodes (carbon fabric electrode and the VNT-CF electrode). The coin cell fabricated with theVNT-CF electrode delivers maximum energy density of 11.6 W h kg^{-1} and 1200 W K g^{-1} of power density at discharge current densities at 0.1 and 1.0 A g^{-1}, respectively. Even at high discharge current rates, the low potential drop (iR drop) at the beginning of the discharge suggests a lower internal resistance. It should be noted that the VNT-CF electrode delivers a higher energy density due to the redox active V_2O_5 nanotubes and the spherical morphology. Electronic contact of VNTs not only to the substrate but also between nanotubes could enhance the power performance as V_2O_5 has poor electronic conductivity. In spite of the power density, the VNT structures display long cycling life. Figure 7 shows the 50 continuous cycles obtained at 5 mVs^{-1}. The area of each cycle is proportional to the amount of Li^+ intercalated. Higher current output and constant cyclic performance explains the stability of VNT clusters toward intercalation/deintercalation of Li^+ ions. The almost constant current output of the cyclic voltammograms recorded up to 50 cycles demonstrates the stability of VNT clusters toward long-term cycle charging and discharging.

CONCLUSION

Vanadium oxide nanotube clusters having densely packed nanotubes in radial arrangement were prepared on high-surface-area carbon fiber fabric (Spectracarb) via pulsed laser deposition followed by hydrothermal treatment. High-surface-area carbon fibers serve as the conducting material and freestanding substrate for the VNT clusters prepared by hydrothermal synthesis. SEM images clearly show the micrometer size spherical clusters consist of densely packed nanotubes. The TEM images further confirmed the formation of a tubular structure having inner, outer diameters and interlayer distances of ~24, ~70, and ~2.4 nm, respectively. Test cells were assembled (CR2032 coin cells) in two electrode configuration and the performance of the VNT-CF electrode as the anode material was studied. The VNT-CF electrodes exhibit promising electrochemical properties suitable for energy storage applications with long-term stability during charge and discharge cycles. These VNT spherical clusters on carbon fabrics exhibit an energy density of 11.6 W h kg^{-1} and power density of 1.2 kW K g^{-1}.

AUTHOR INFORMATION

Corresponding Author
*E-mail: balkus@utdallas.edu.

ACKNOWLEDGMENT

We acknowledge the U.S. Department of Energy (DE-EE004186) for financial support.

REFERENCES

(1) Winter, M.; Brodd, R. J. *Chem. Rev.* **2004**, *104*, 4245.
(2) Hou, Y.; Cheng, Y.; Hobson, T.; Liu, J. *Nano Lett.* **2010**, *10*, 2727.
(3) Yuan, C.; Zhang, X.; Su, L.; Gao, B.; Shen, L. *J. Mater. Chem.* **2009**, *19*, 5772.
(4) Cheng, Q.; Tang, J.; Ma, J.; Zhang, H.; Shinya, N.; Qin, L.-C. *Carbon* **2011**, *49*, 2917.
(5) Bonso, J. S.; Rahy, A.; Perera, S. D.; Nour, N.; Seitz, O.; Chabal, Y. J.; Balkus, K. J.; Ferraris, J. P.; Yang, D. J. *J. Power Sources* **2011**.
(6) Liu, X.; Pickup, P. *J. Solid State Electrochem.* **2010**, *14*, 231.
(7) Zhou, C.; Mai, L.; Liu, Y.; Qi, Y.; Dai, Y.; Chen, W. *J. Phys. Chem. C* **2007**, *111*, 8202.
(8) Wang, Y.; Takahashi, K.; Shang, H.; Cao, G. *J. Phys. Chem. B* **2005**, *109*, 3085.
(9) Ahmad, A.; Koohestani, B.; Bhatia, S.; Ooi, B. *J. Sol−Gel Sci. Technol.* **2010**, *56*, 327.
(10) Xiong, C; Aliev, A. E.; Gnade, B.; Balkus, K. J., Jr. *ACS Nano* **2008**, *2*, 293.
(11) Wang, Y.; Zhang, H.; Lim, W.; Lin, J.; Wong, C. *J. Mater. Chem.* **2011**, *21*, 2362.
(12) Wang, Y.; Takahashi, K.; Lee, K.; Cao, G. *Adv. Funct. Mater.* **2006**, *16*, 1133.
(13) Muhr, H.-J.; Krumeich, F.; Schölzer, U. P.; Bieri, F.; Niederberger, M.; Gauckler, L. J.; Nesper, R. *Adv. Mater.* **2000**, *12*, 231.
(14) Liu, A.; Ichihara, M.; Honma, I.; Zhou, H. *Electrochem. Commun.* **2007**, *9*, 1766.
(15) Chan, C.; Peng, H.; Twesten, R.; Jarausch, K.; Zhang, X.; Cui, Y. *Nano Lett.* **2007**, *7*, 490.
(16) Gloskovskii, A.; Nepijko, S.; Schönhense, G.; Therese, H.; Reiber, A.; Kandpal, H.; Fecher, G.; Felser, C.; Tremel, W.; Klimenkov, M. *J. Appl. Phys.* **2007**, *101*, 084301(1−6).
(17) O'Dwyer, C.; Lavayen, V.; Tanner, D. A.; Newcomb, S. B.; Benavente, E.; González, G.; Torres, C. M. S. *Adv. Funct. Mater.* **2009**, *19*, 1736.
(18) Velazquez, J.; Banerjee, S. *Small* **2009**, *5*, 1025.
(19) Ceccato, R.; Dirè, S.; Barone, T.; De Santo, G.; Cazzanelli, E. *J. Mater. Res.* **2009**, *24*, 475.
(20) Mohan, V.; Hu, B.; Qiu, W.; Chen, W. *J. Appl. Electrochem.* **2009**, *39*, 2001.
(21) Navone, C.; Baddour-Hadjean, R.; Pereira-Ramos, J.; Salot, R. *Electrochim. Acta* **2008**, *53*, 3329.
(22) Ramana, C.; Hussain, O.; Naidu, B.; Reddy, P. *Thin Solid Films* **1997**, *305*, 219.
(23) Barreca, D.; Armelao, L.; Caccavale, F.; Di Noto, V.; Gregori, A.; Rizzi, G.; Tondello, E. *Chem. Mater.* **2000**, *12*, 98.
(24) McGraw, J.; Perkins, J.; Hasoon, F.; Parilla, P.; Warmsingh, C.; Ginley, D.; Mateeva, E.; Readey, D. *J. Mater. Res.* **2000**, *15*, 2249–2265.
(25) Ramana, C.; Smith, R.; Hussain, O.; Chusuei, C.; Julien, C. *Chem. Mater.* **2005**, *17*, 1213.
(26) Perera, S.; Balkus, K., Jr. *Mater. Res. Soc. Symp. Proc.* **2010**, *1211*, 115.
(27) Balkus, K., Jr.; Gbery, G.; Deng, Z. *Microporous Mesoporous Mater.* **2002**, *52*, 141.
(28) Fang, G.; Liu, Z.; Wang, Y.; Liu, H.; Yao, K. *J. Phys. D: Appl. Phys.* **2000**, *33*, 3018.
(29) Julien, C.; Haro-Poniatowski, E.; Camacho-López, M.; Escobar-Alarcón, L.; Jímenez-Jarquín, J. *Mater. Sci. Eng., B* **1999**, *65*, 170.
(30) Iida, Y.; Kanno, Y. *Jpn. J. Appl. Phys.* **2008**, *47*, 667.
(31) Liu, H.; Wang, Y.; Li, H.; Yang, W.; Zhou, H. *ChemPhysChem.* **2010**, *11*, 3273.
(32) Fei, H.; Shen, Z.; Wang, J.; Zhou, H.; Ding, D.; Chen, T. *J. Power Sources* **2009**, *189*, 1164.
(33) O'Dwyer, C.; Navas, D.; Lavayen, V.; Benavente, E.; Santa Ana, M.; González, G.; Newcomb, S.; Sotomayor Torres, C. *Chem. Mater.* **2006**, *18*, 3016.
(34) Kim, Y.; Kim, J.-S.; Thieu, M.-T.; Dinh, H.-C.; Yeo, I.-H.; Cho, W.; Mho, S.-I. *Bull. Korean Chem. Soc.* **2010**, *31*, 3109.
(35) Li, Z.; Ruckenstein, E. *Langmuir.* **2002**, *18*, 6956.
(36) Chen, Z.; Qin, Y.; Weng, D.; Xiao, Q.; Peng, Y.; Wang, X.; Li, H.; Wei, F.; Lu, Y. *Adv. Funct Mater.* **2009**, *19*, 3420.
(37) Wang, Y.; Li, H.; He, P.; Hosono, E.; Zhou, H. *Nanoscale.* **2010**, *2*, 1294.
(38) Perera, S. D.; Patel, B.; Nijem, N.; Roodenko, K.; Seitz, O.; Ferraris, J. P.; Chabal, Y. J.; Balkus, K. J. *Adv. Energy Mater.*, Wiley-VCH: Weinheim, Germany, 2011; Vol. 1, p 936.
(39) Fang, W.-C.; Fang, W.-L. *Chem. Commun.* **2008**, 5236.

(40) Chen, L.-M.; Lai, Q.-Y.; Hao, Y.-J.; Zhao, Y.; Ji, X.-Y. *J. Alloys Compd.* **2009**, *467*, 465.
(41) Grigor'eva, A.; Anikina, A.; Tarasov, A.; Gudilin, E.; Knot'ko, A.; Volkov, V.; Dembo, K.; Tret'yakov, Y. *Dokl Chem.* **2006**, *410*, 165.
(42) Mai, L.; Chen, W.; Xu, Q.; Zhu, Q.; Han, C.; Peng, J. *Solid State Commun.* **2003**, *126*, 541.
(43) Avansi, W., Jr.; Ribeiro, C.; Leite, E.; Mastelaro, V. *Cryst. Growth Des.* **2009**, *9*, 3626.
(44) Shen, Y.; Peng, L.; Guo, X.; Ding, W. *Chem. Lett.* **2009**, *38*, 928.
(45) Liu, A.; Ichihara, M.; Honma, I.; Zhou, H. *Commun.* **2007**, *9*, 1766.
(46) Krumeich, F.; Muhr, H.-J.; Niederberger, M.; Bieri, F.; Schnyder, B.; Nesper, R. *J. Am. Chem. Soc.* **1999**, *121*, 8324.
(47) Fang, W.-C. *J. Phys. Chem. C.* **2008**, *112*, 11552.
(48) Liu, X.; Huang, C.; Qiu, J.; Wang, Y. *Appl. Surf. Sci.* **2006**, *253*, 2747.
(49) Decker, F.; Donsanti, F.; Salvi, A.; Ibris, N.; Castle, J.; Martin, F.; Alamarguy, D.; Vuk, A.; Orel, B.; Lourenco, A. *J. Braz. Chem. Soc.* **2008**, *19*, 667.